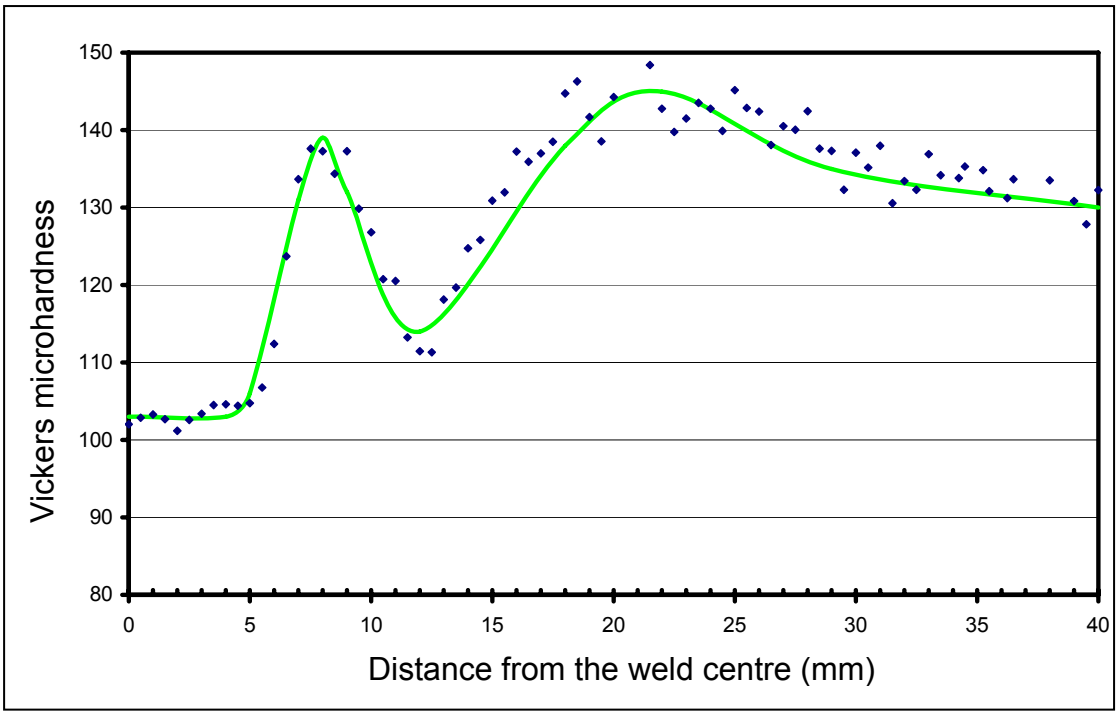

Fig.1 Hardness as a function of the distance from the weld centre (at 0 mm) of the VPPA welds with numbered positions for microstructural examination. Error bars indicate estimated accuracy of sample extraction.

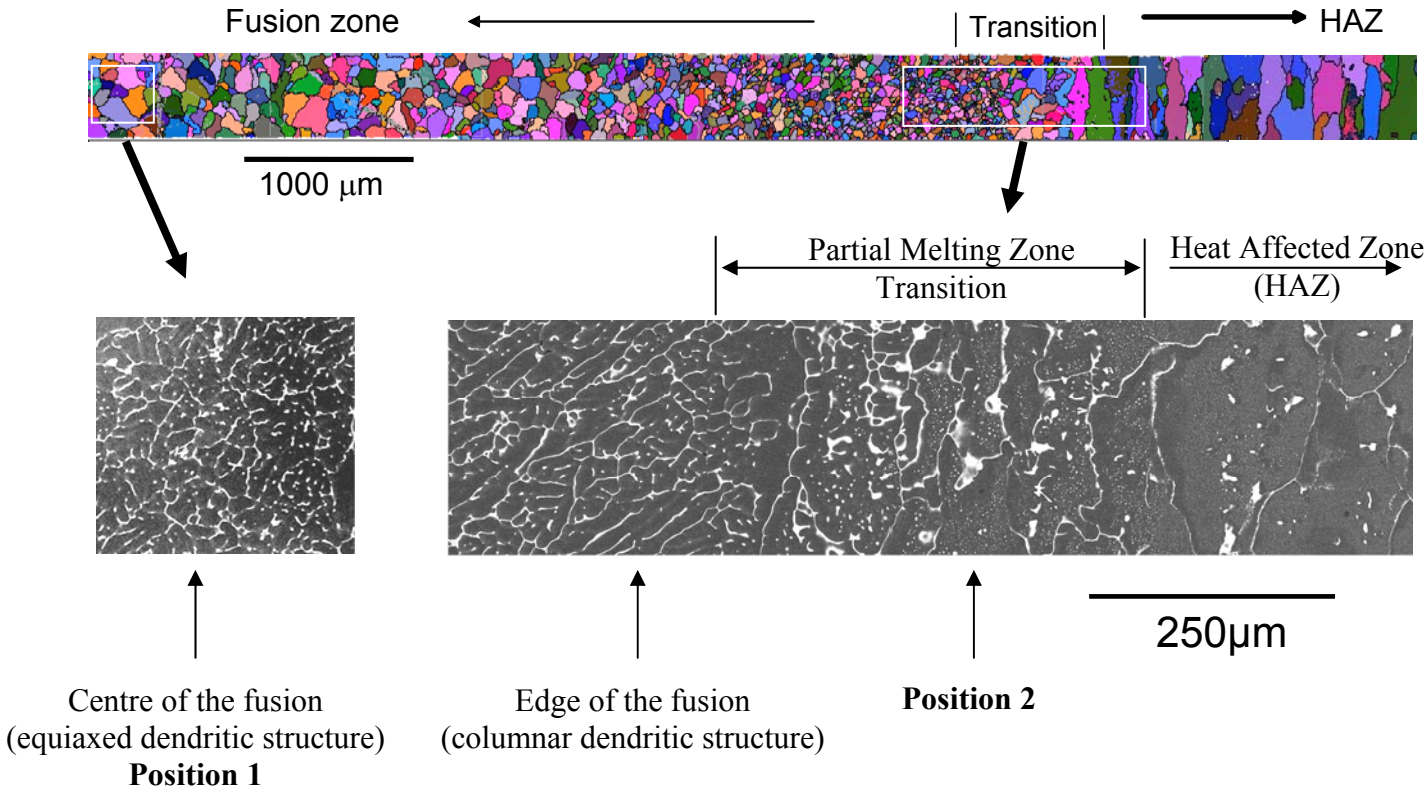

Fig. 2 EBSD orientation map showing high angle grain boundary distribution in fusion zone and partial heat affected zone. The lower two figures are backscattered electron FEG-SEM images of the fusion zone (square frame) and transition zone (rectangle frame).

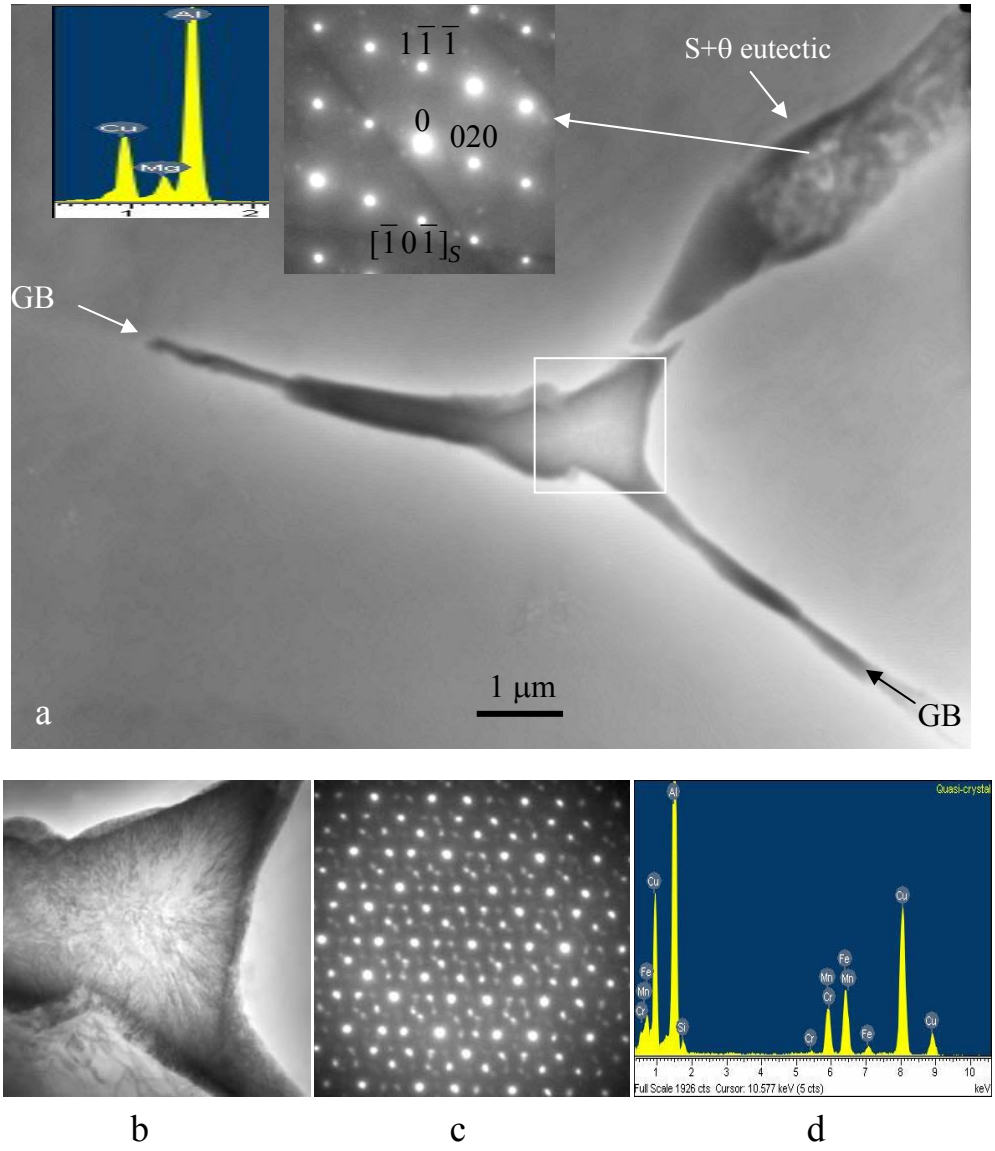

Fig. 3a TEM micrograph showing eutectic phases primarily as dendritic grains and icosahedral phases on the grain boundaries in position 1 (melting zone). The dendritic phases were confirmed as θ+S eutectic phases by EDS and SAD pattern (inserts).

b The enlargement of the GB phase on frame of a. The SAD pattern shows an icosahedral structure with composition determined as close to $Al_7Cu_2(Fe,Mn)$ (from the EDS data in (d))

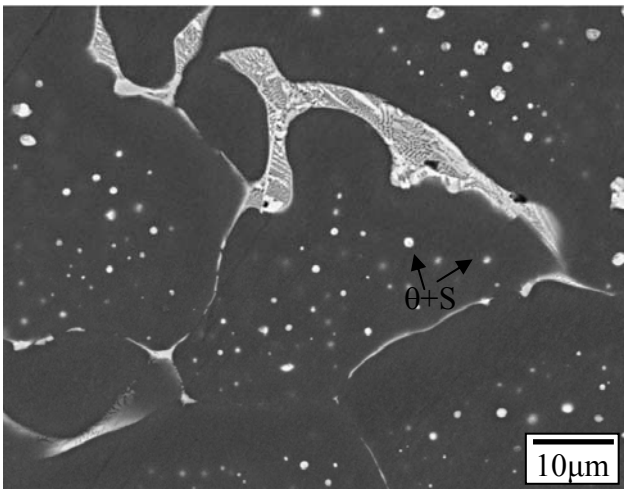

Fig. 4 High magnification SEM backscattered electron image of the partial melting zone.

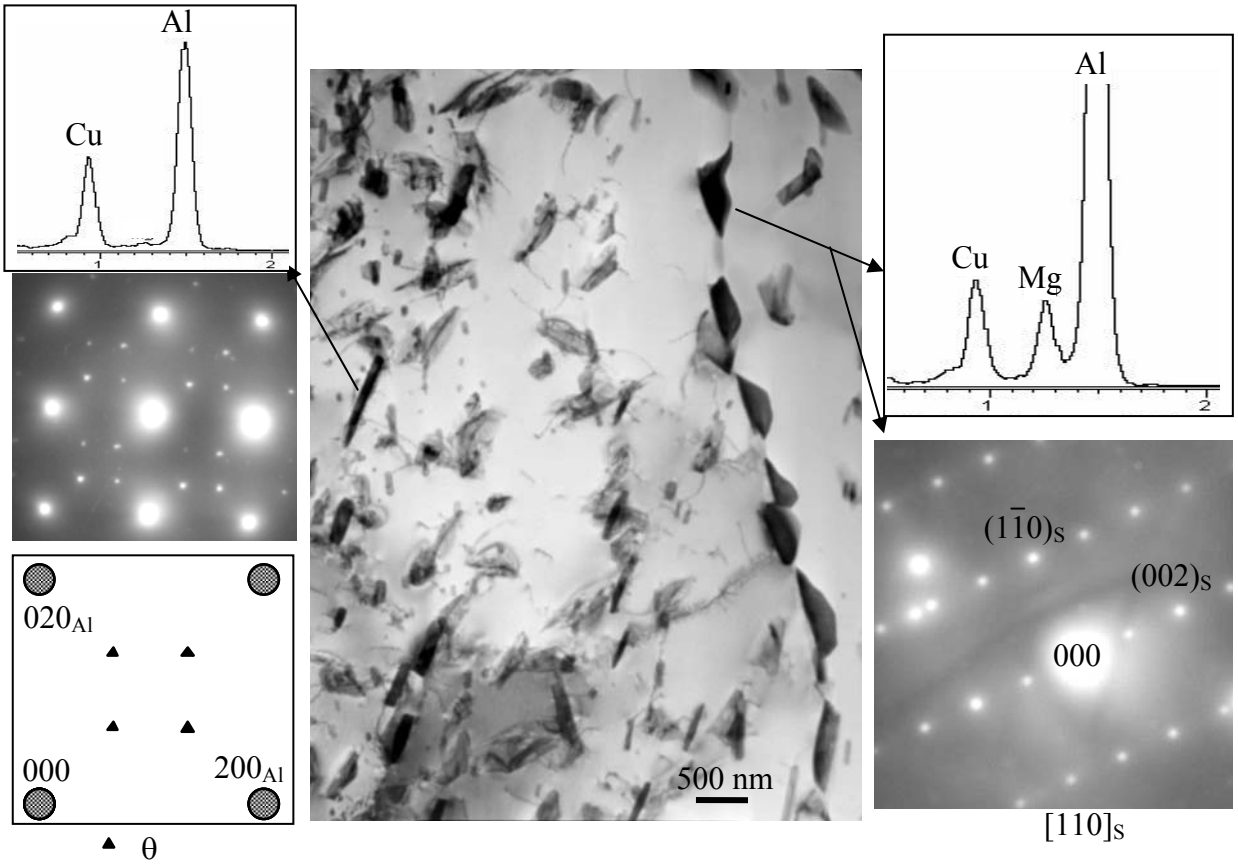

Fig. 5 The large θ precipitates formed at Position 2 (re-solutionising zone), with S formed on a HAGB. The left figure clusters show EDS chemical analysis for one of θ precipitates, SAD pattern and the corresponding schematic diagram on $[001]_{Al}$. The right figure clusters show EDS chemical analysis, the corresponding diffraction pattern and the corresponding schematic diagram on $[110]_S$ for one of S phase in a high angle grain boundary.

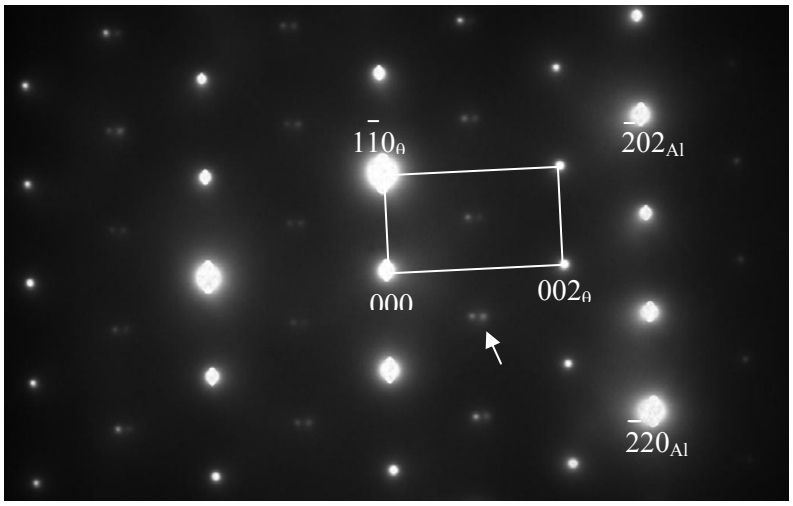

Fig. 6 The SAD pattern close to $[111]_{Al}$. Some weak reflections are clearly split as the c lattice parameter of θ phase is not perfect matching with aluminium matrix.

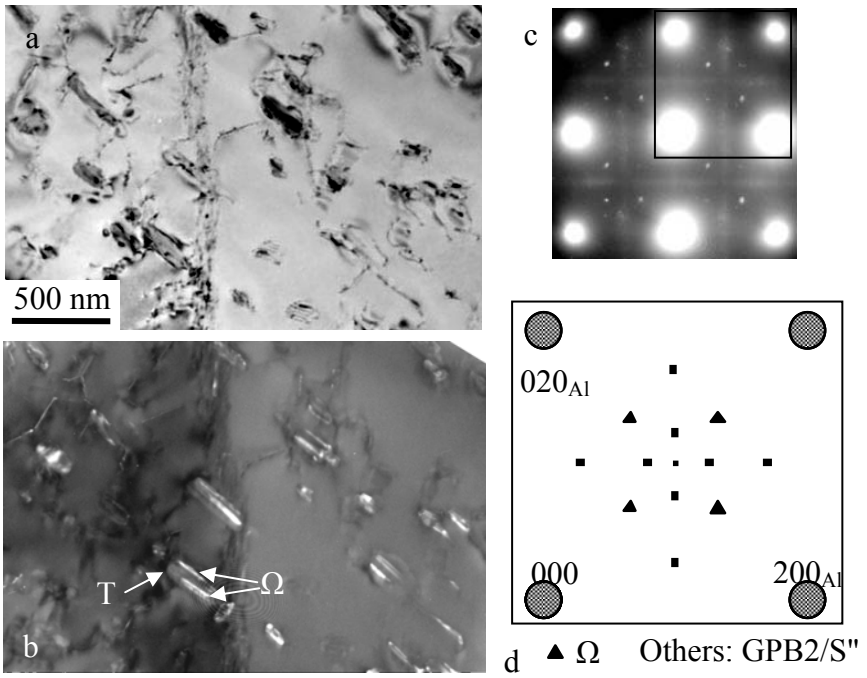

Fig. 7 The Ω precipitates at position 3. Some Ω formed around rod particles (T-$Al_{20}Cu_2Mn_3$).

a. Bright field image
b. Dark field image; One sandwich phases were indicated by T phase inside and Ω precipitates outside.
c. SAD pattern $[001]_{Al}$.
d. The schematic diagram indicating the formation of Ω precipitates and GPB2/S". The latter phase, however, cannot be resolved by conventional TEM

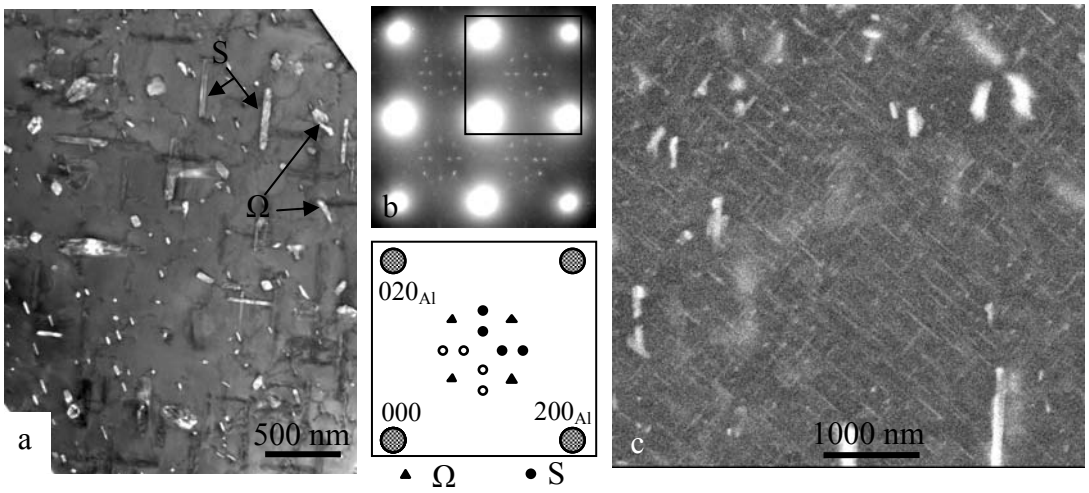

Fig. 8a. The dark field image of Ω and S precipitates along $[001]_{Al}$ in position 4. Fig. 8b shows the corresponding diffraction pattern and schematic diagram. The S phase is in the coarsening stage, in which S precipitates may see in the high resolution SEM as shown in Fig. 8c.

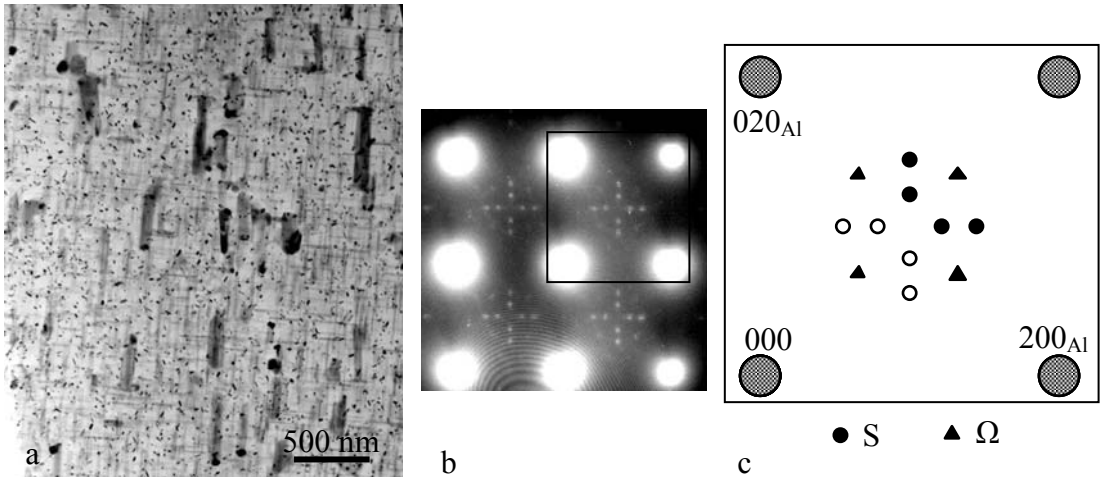

Fig. 9a. The bright field image of Ω and S precipitates along $[001]_{Al}$ in position 5. The SAD and schematic diagram are shown in Fig. 9b and 9c.

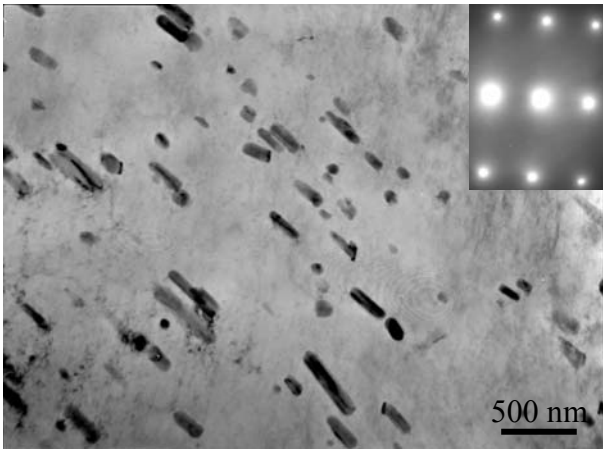

Fig. 10 TEM micrograph (bright field) of the matrix in position 6. The diffraction pattern (insert) does not show any evidence of the existence of precipitates.

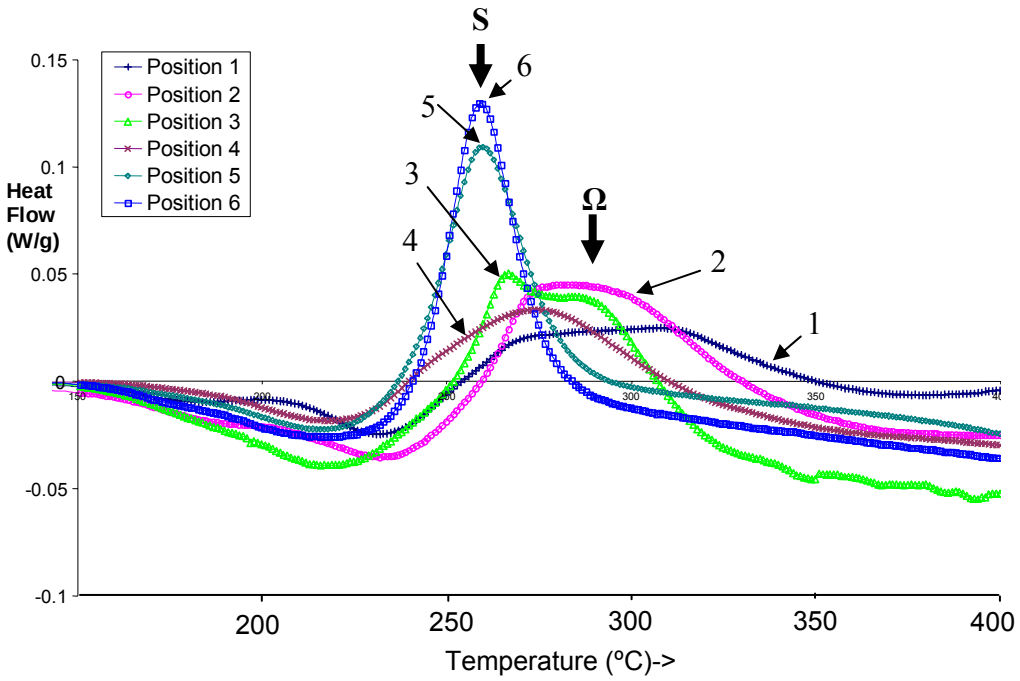

Fig. 11 DSC thermograms for the various curve locations highlighted in Fig.1

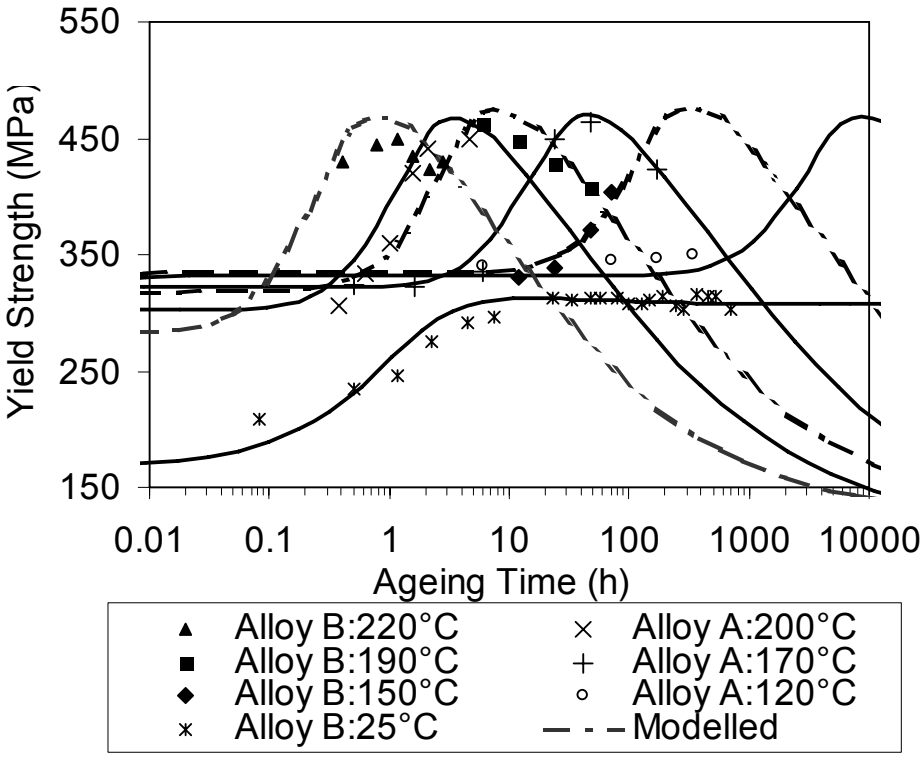

Fig. 12 Predicted and measured strength evolution for an Al-4.2Cu-1.36Mg-0.58Mn-0.08Fe –0.06Si (wt%) alloy (A) and an Al-4.34Cu-1.37Mg-0.42Mn-0.08Fe-0.05Si (wt%) alloy (B). For ageing at 25°C and 220°C hardness data is converted to yield strength using YS=3Hv for 220°C curve and YS=2.3Hv for 25°C curve.

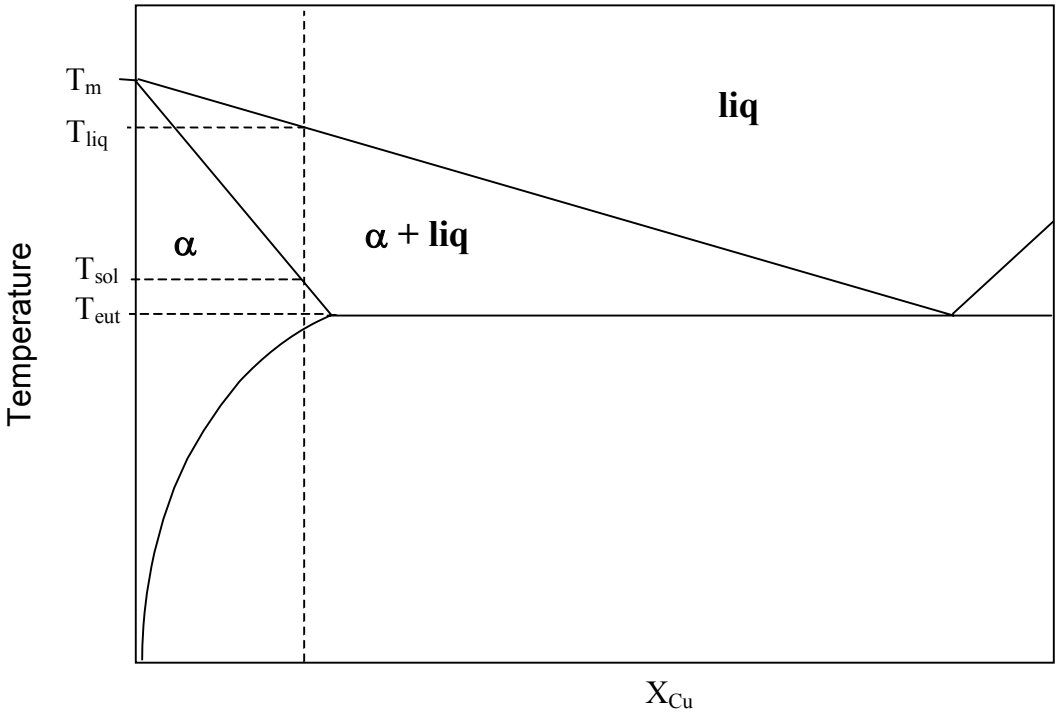

Fig. 13 Portion of a schematic, pseudo-binary phase diagram used for calculation the amount of Cu dissolved in the Al-rich phase on partial melting.

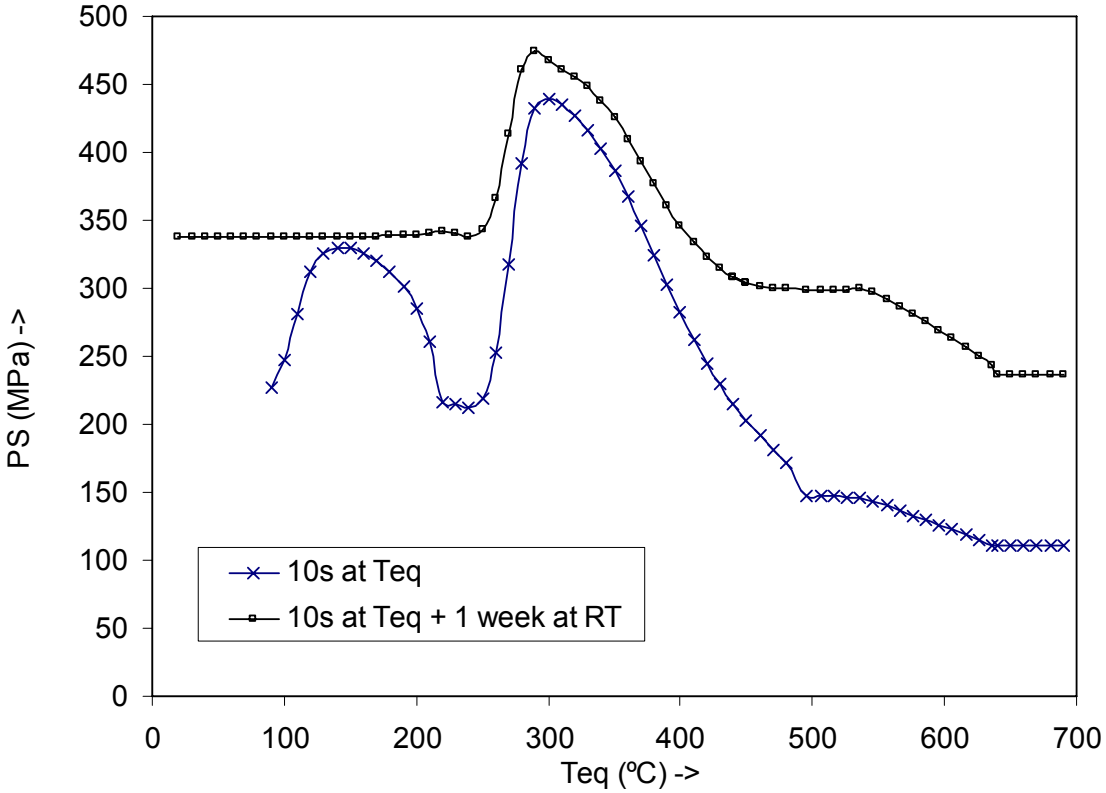

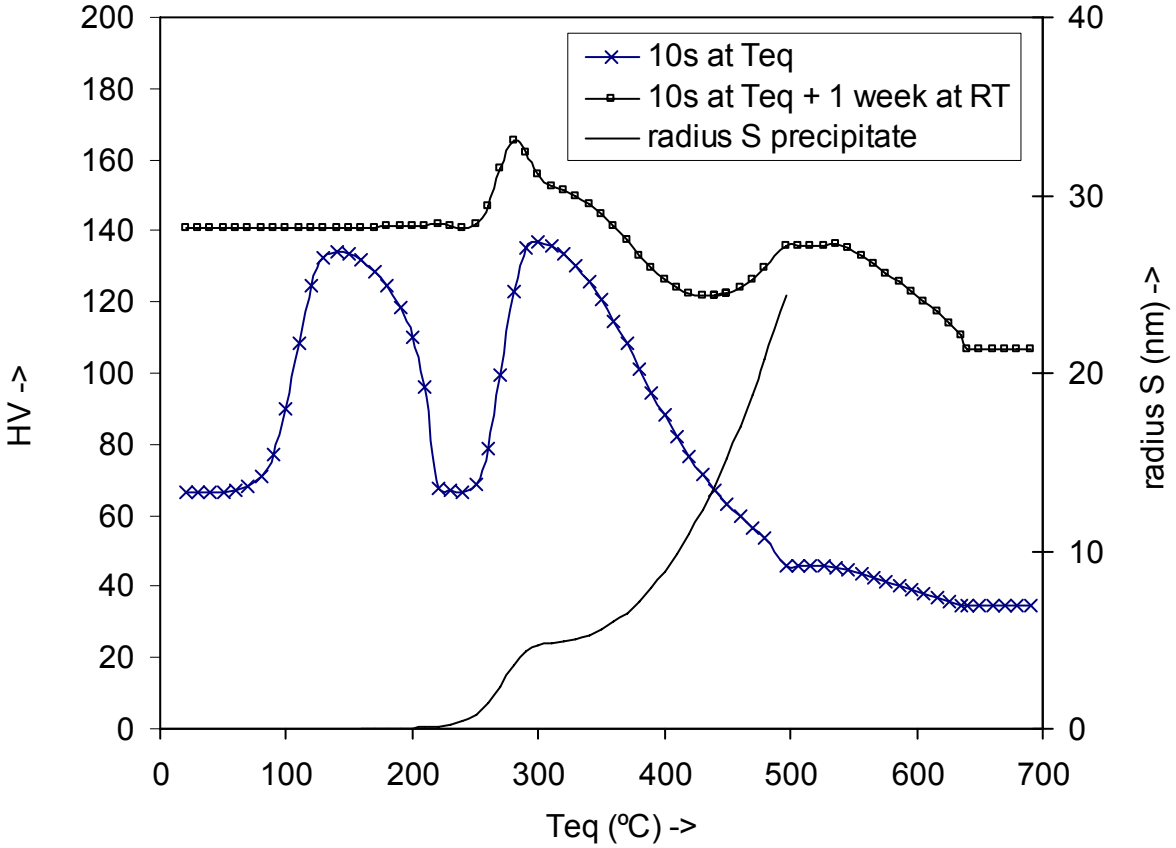

Fig. 14 Model predictions of proof strength (a) and hardness (b) in the heat effected zone and weld as a function of the maximum equivalent temperature reached in the heat effected zone. The lower curve is the prediction for strength after a hypothetical rapid cooling from T_{eq} and the top curve is the prediction for strength after exposure at T_{eq} followed by extensive room temperature ageing. In (b) the predicted radius of the rod-shaped S phase precipitates is also plotted.

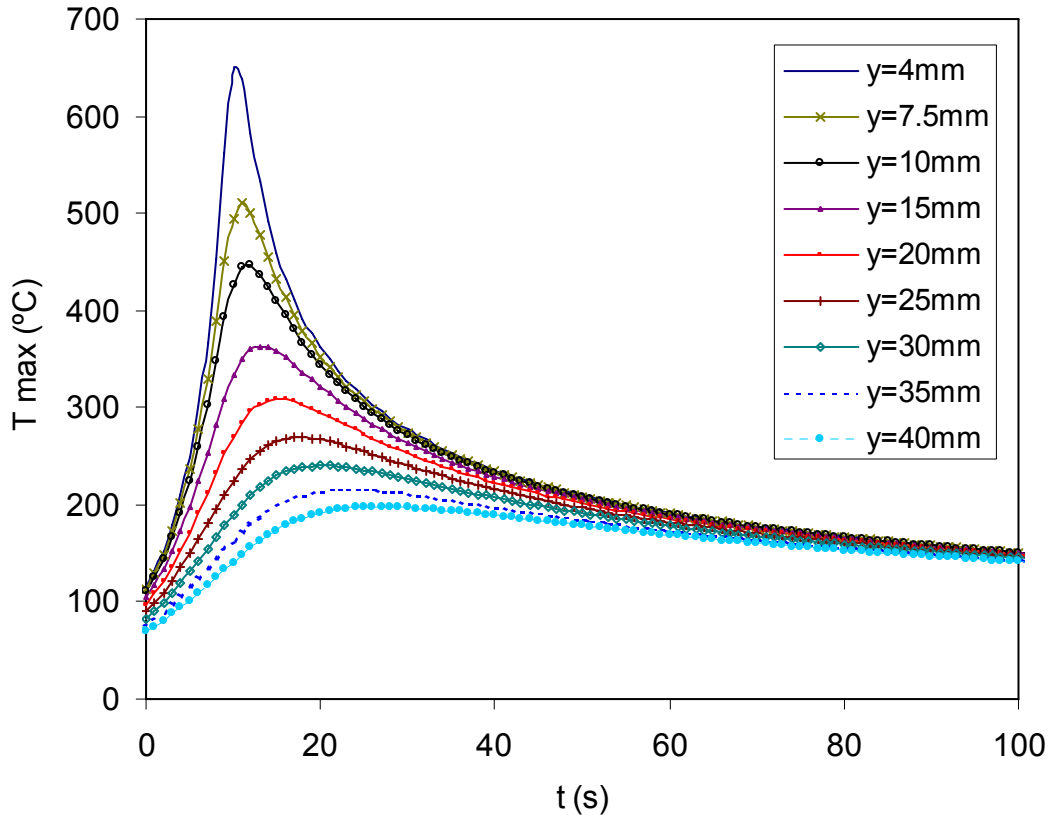

Fig. 15 Predicted temperatures from the 2D heat diffusion model.

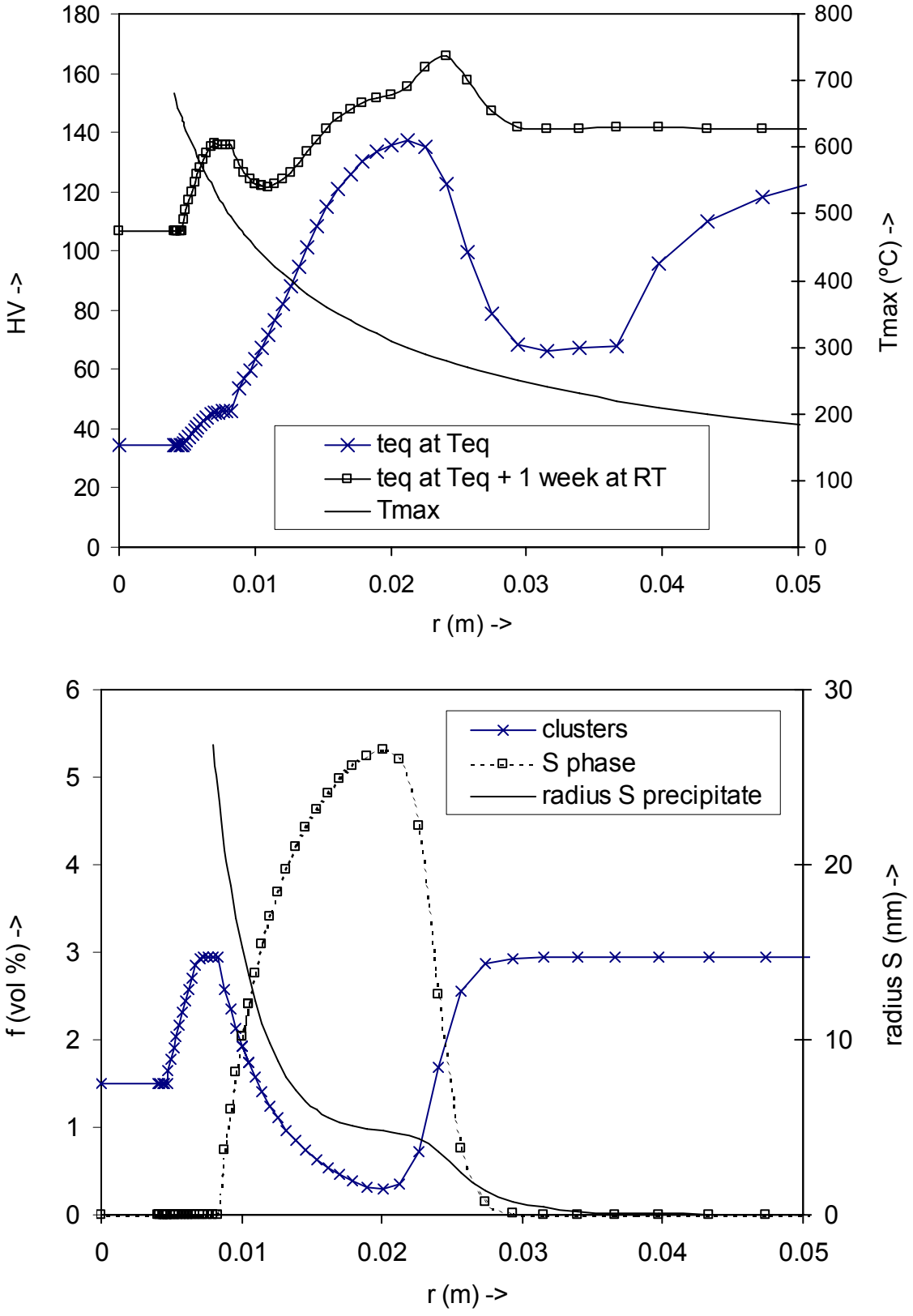

Fig. 16 Model predictions of hardness (a) and volume fraction of precipitates (b) as a function of the distance to the weld centre line. In (a) the lower curve is the prediction for hardness after a hypothetical rapid cooling from T_{eq} and the top curve is the prediction for hardness after exposure at T_{eq} followed by extensive room temperature ageing. Also plotted is the predicted radius of the rod-shaped S phase precipitates.

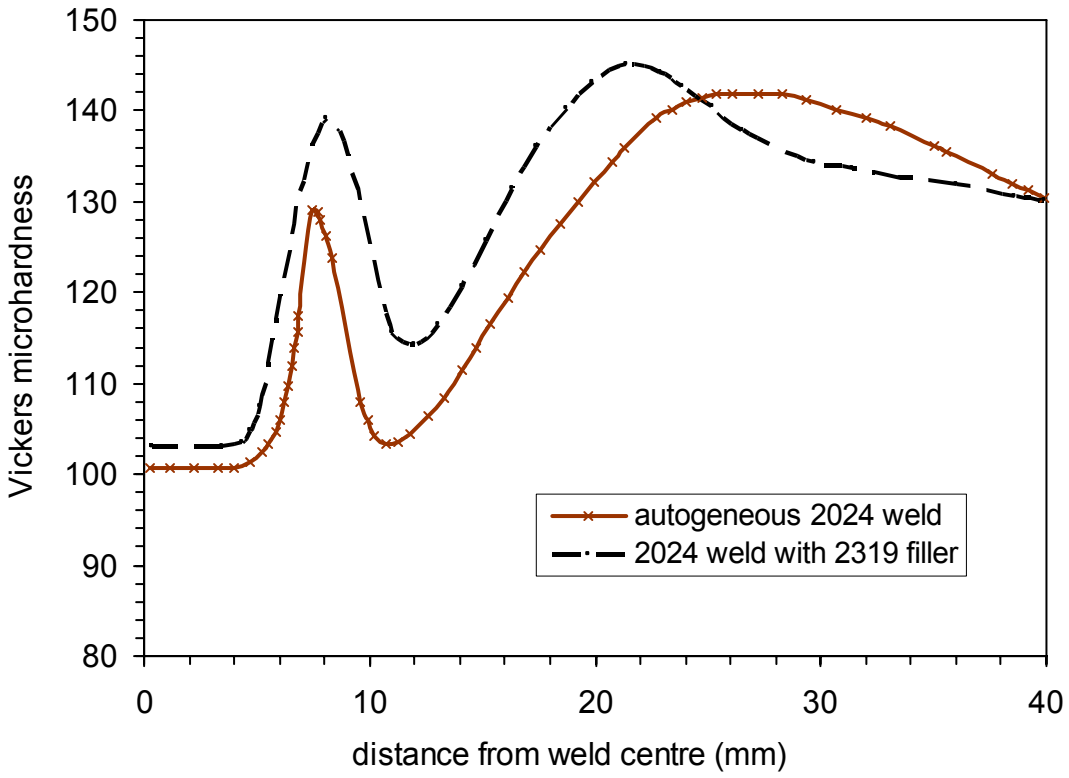

Fig. 17 Representative hardness traces for the top surface of the filled VPPA and autogeneous VPPA welds.